

Research Paper

Rhomboedric Cassiterite as Inclusions in Tetragonal Cassiterite from Slavkovský les – North Bohemia (Czech Republic)

Rainer Thomas*

Im Waldwinkel 8, D-14662 Friesack, Germany

*Corresponding author: Rainer Thomas, Im Waldwinkel 8, D-14662 Friesack, Germany

Received: July 11, 2024; Accepted: July 16, 2024; Published: July 20, 2024

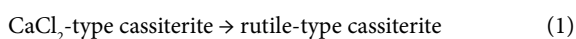
Abstract

In this contribution, we show the existence of the orthorhombic high-pressure CaCl_2 -type cassiterite included as inclusions in rutile-type cassiterite from Slavkovský les. The proof of the existence of orthorhombic CaCl_2 -type cassiterite demands a pressure of 12–15 GPa or more for the formation, corresponding to a deep of about 560 km. Furthermore, the transport from that deep to the crust level must be speedy to prevent the high-pressure phases from destruction at lower temperatures and pressures.

Keywords: CaCl_2 -type to rutile-type cassiterite, Raman spectroscopy, Phase transitions, Supercritical fluid, Fast transport from the mantle to crust

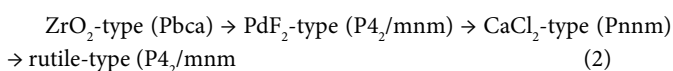
Introduction

Besides the meaning of cassiterite as an essential ore mineral, Sn oxide has received a lot of attention (see Balakrishnan et al. (2022) [1] as popular gas sensors, and according to Gupta et al. (2013) as solar cells, optoelectronic devices, oxidation catalyst, etc. Cassiterite crystallizes in nature generally in the tetrahedral class in the space group $P4_2/mnm$ (rutile type). There are also different polymorphs in nature and different polytypes synthetically produced by experimental research. Balakrishnan et al. (2022) – [1] have investigated the structure stability and properties of 20 SnO_2 polymorphs. The most common phase transition of the rutile-type cassiterite under pressure is the transformation into the orthorhombic (Pnnm) CaCl_2 -type cassiterite (Gupta et al. 2013) – [2] because both structures are closely related. In nature, of course, the transformation happens in the reverse direction:



The transformation pressure is around 12 GPa [3].

The complete sequence of phase transitions, determined with x-ray techniques, is, according to the same authors [3], from high to low pressure (space groups in brackets):



The transformation pressures are 50, 20, and 12 GPa, respectively.

Here, we will present a second natural example of the transformation of the high-pressure CaCl_2 -type cassiterite into low-pressure tetragonal cassiterite [4]. The remnants of high-pressure cassiterite in more crustal low-pressure cassiterite require fast

transport from mantle depths to a more crustal regime, probably by supercritical fluids/melts to prevent the complete transition from CaCl_2 -type into the rutile type cassiterite. The motivation for the present study is to show that besides the found high-pressure non-ore minerals (diamond, lonsdaleite, graphite, moissanite, high-pressure beryl, stishovite, coesite, cristobalite-X-1 [4-6] also ore minerals like cassiterite can store information of the complex pressure history.

Sample Material

In the Sn–W mineralization from the Slavkovský les, there are three principal mineralization types: (1) disseminated-type mineralization, (2) ore pockets, and (3) quartz veins. The disseminated mineralization has a typical content of 0.2–0.3 [% (g/g)] Sn. The ore pockets are rounded or even deformed irregular bodies tens of centimeters in size, with a very high proportion of cassiterite. The studied samples come from type 2 (pockets) and are old samples from the State Mineral Collection (Niederlage) of the Mining Academy Freiberg. The studied cassiterite crystals have a diameter of about 2 cm. Most both-side polished thick sections (about 500 μm thick) of such cassiterite show under the crossed Nicols different amounts of birefringent grains (often rounded) of orthorhombic cassiterite crystals. Some are very small as they are glowing grains like a starry sky (Figure 1a). Counting of such about 1–2 μm -large orthorhombic crystals gives 4×10^6 inclusions per cubic centimeter. Larger crystals are from about 55 \times 45 μm to 300 \times 170 μm large (Figures 2 and 3). The thermometric data of the used samples from the Slavkovský les are in Thomas (1982) [7]: Sn-6, Sn-28, Sn-30, Sn-44, and Sn-45. All five samples contain orthorhombic cassiterite inclusions in rutile-type cassiterite as host.

Some cassiterite crystals (e.g., Sn-49 contain tiny diamond crystals with the characteristic Raman band at 1330.9 cm^{-1} (Figure 1b) deep in

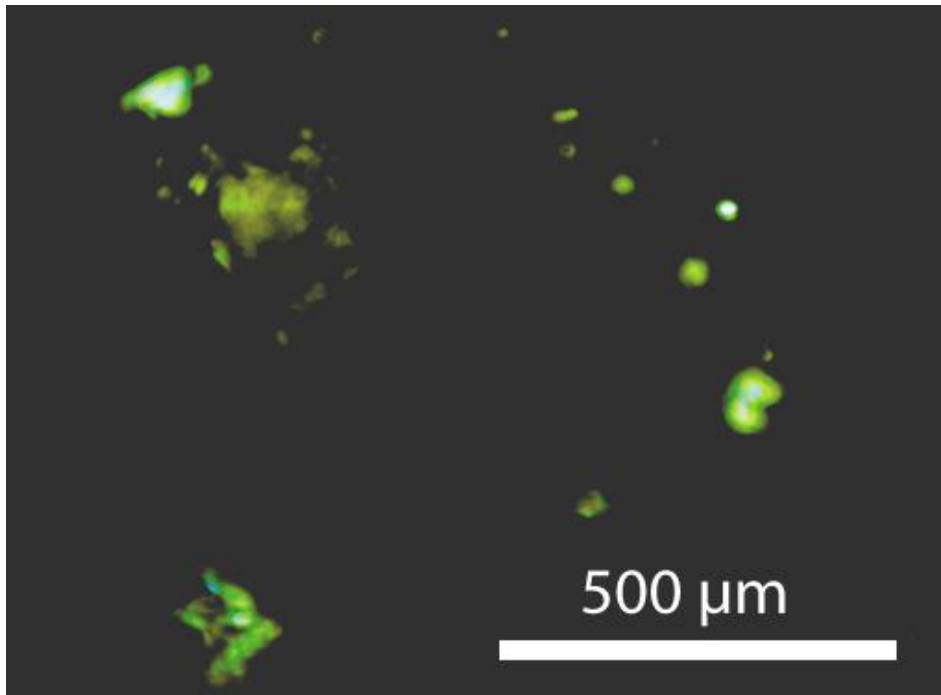


Figure 1a: Tetragonal rutile-type cassiterite (black) with remnants of CaCl₂-type (o-Cst) cassiterite inclusions (bright) distributed through the whole crystal under crossed Nicols.

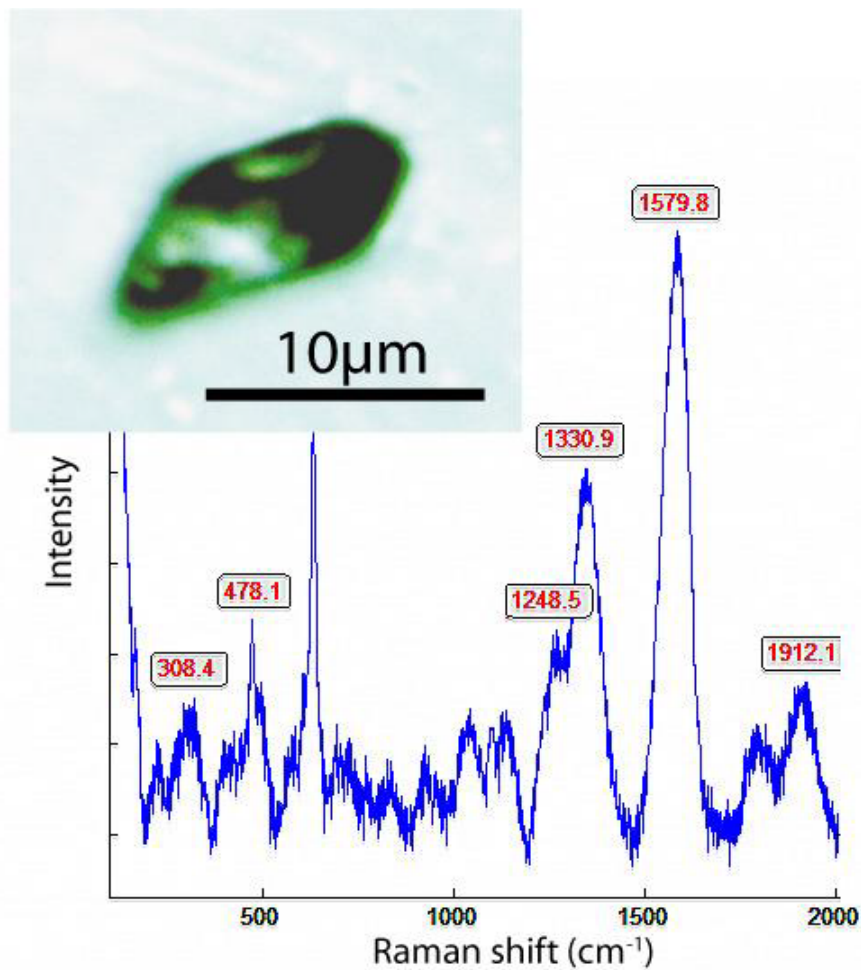


Figure 1b: Raman spectrum of diamond in rutile-type cassiterite (Sn-49) from Slavkovský les. The inserted photomicrography shows an about 12 μm long diamond (+ graphite) crystal in that cassiterite.

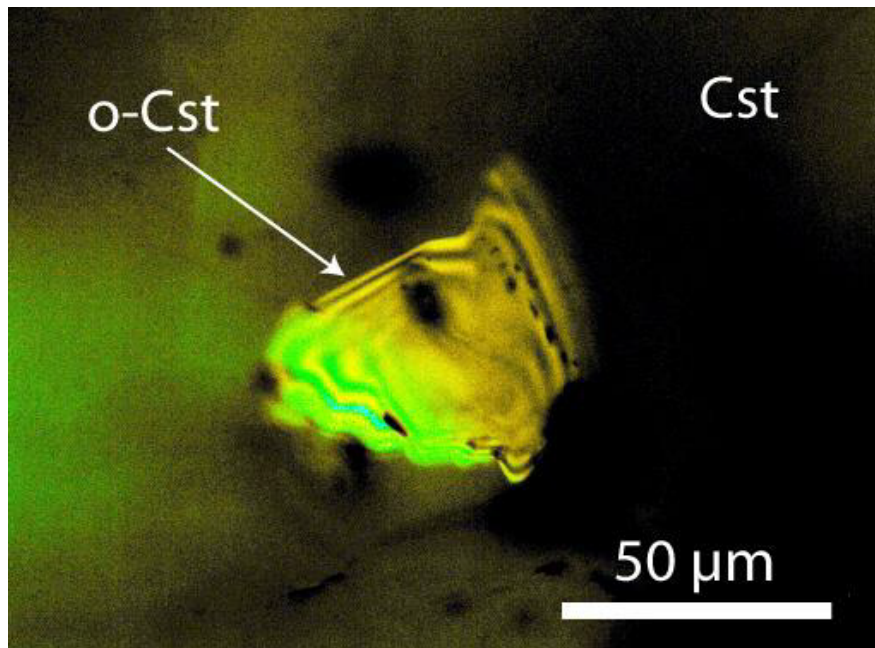


Figure 2: Single orthorhombic (o-Cst) cassiterite crystal in tetragonal cassiterite from Slavkovský les.

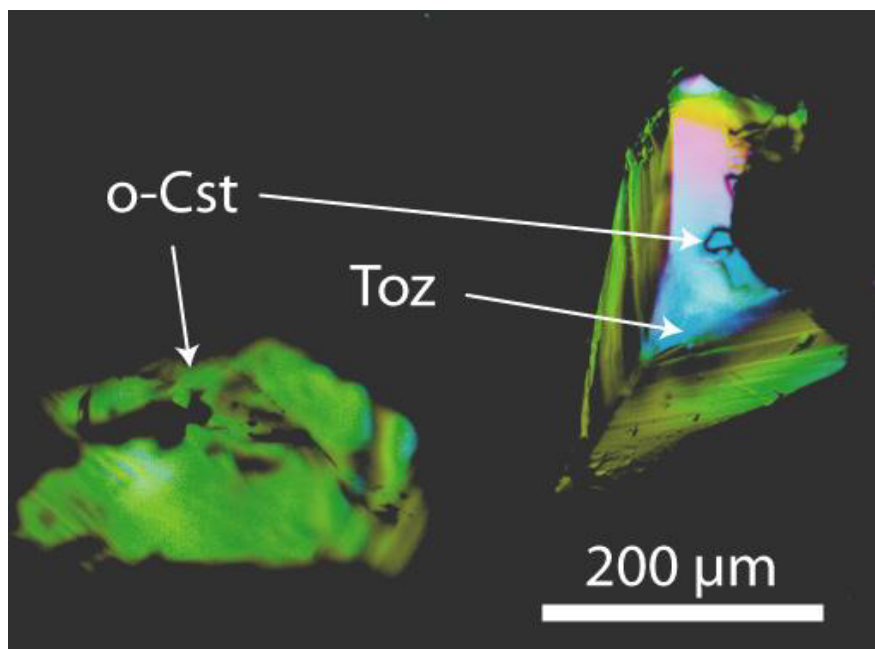


Figure 3: Tetragonal rutile-type cassiterite (black) from Slavkovský les with topaz (Toz) and CaCl_2 -type (o-Cst) cassiterite inclusions under crossed Nicols. The topaz crystal contains a small o-Cst crystal in the center.

the volume (not at or near the surface) – see Thomas et al. 2023 [8]. Graphite (Raman band at 1580 cm^{-1}) is oft present (here in diamond) in the cassiterite from the Variscan tin deposits of the Erzgebirge/Krušné hory and Slavkovský les, demonstrating more reducing conditions in the early stage.

In the form of larger crystals (10 to $300\text{ }\mu\text{m}$), the orthorhombic cassiterite (CaCl_2 -type) is under the microscope and crossed Nicols good to see in the tetragonal rutile-type cassiterite matrix.

Microscopy and Raman Spectroscopy: Methodology

For the study of the cassiterite samples and their paragenetic main minerals, we use the Zeiss JENALAB pol as well as the Raman spectrometer EnSpectr R532 combined with the Olympus BX43 microscope both for transmitted and reflected light and equipped with a rotating stage and polarizers (for parallel and perpendicular positions). Note here that the incident laser light is always polarized – in our case, N – S [9]. Generally, we used an Olympus long-distance LMPLFL100x objective lens for the principal studies. For the identification of different minerals, we used the RRUFF and the Hurai et al. Raman mineral databases [10,11]. As references, we applied a

water-clear diamond crystal from Brazil ($1331.63 \pm 0.60 \text{ cm}^{-1}$) and a semiconductor-grade silicon single-crystal ($520.70 \pm 0.15 \text{ cm}^{-1}$). For this study, we generally used laser energies of $\leq 30 \text{ mW}$ on the sample for overview studies and 0.15 mW (1000 s counting time) to prevent heating for exact measurements of the peak positions.

Results

A typical Raman spectrum of orthorhombic cassiterite in the cassiterite host (rutile-type cassiterite) from Slavkovský les is shown in Figure 4.

For comparison, Figure 5 shows a typical Raman spectrum of the rutile-type cassiterite host, which clearly has lesser Raman active bands.

The difference between orthorhombic and tetragonal cassiterite is demonstrated in Figures 4 and 5. In Table 1 are the measured Raman bands of the orthorhombic cassiterite shown (Figure 4).

According to Girão et al. (2018) [3], the intensity of some Raman bands of the CaCl_2 -type cassiterite increases significantly with pressure. From Table 1, we see that the 447 cm^{-1} band is the strongest Raman band in the studied CaCl_2 -type cassiterite.

Table 1: Measured Raman bands of the orthorhombic cassiterite from Slavkovský les (sample Sn-6).

Raman band (cm^{-1})	FWHM (cm^{-1})	Intensity (rel.)	Critical Raman bands (cm^{-1})	Number of measurements	Raman mode
120.8	48.4	35.4	117.8 ± 13.5	56	A_g
165.8	32.4	10.9			
238.6	21.1	5.3			
265.9	86.5	9.5			
446.7	18.1	100	444.8 ± 2.6	56	E_g
469.4	17.6	21.3	470.0 ± 3.9	43	E_g
504.4	41.6	7.1			
577.8	26.5	13.9			
616.4	18.3	10.8			
632.7	11.4	23.8			
637.6	49.3	19.3			
775.0	8.4	2.2			
834.4	18.5	63.5	834.8 ± 0.7	53	B_{1g}
895.7	24.9	7.6			
1279.3	34.8	8.9			

FWHM: Full Width at Half Maximum.

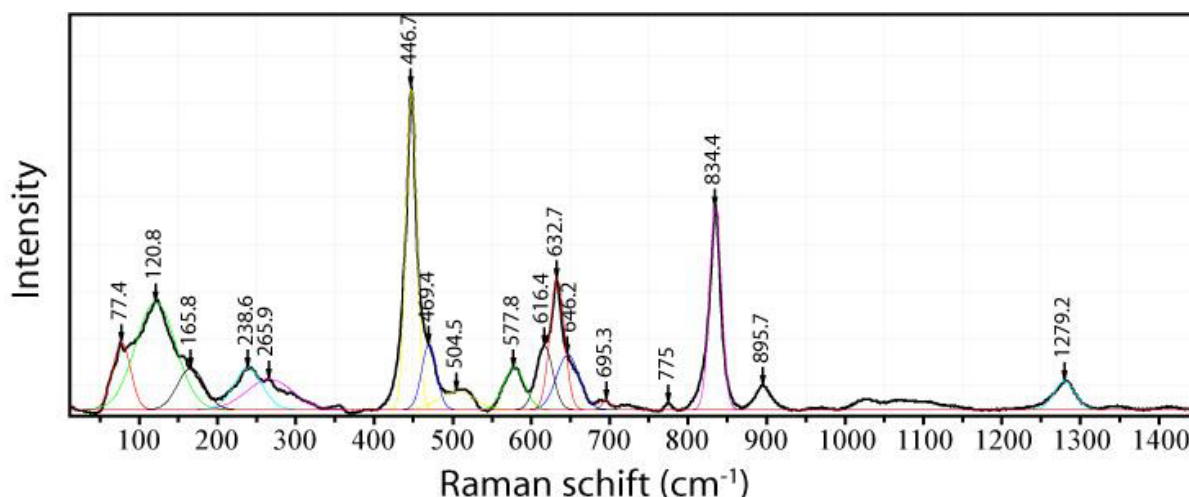


Figure 4: Raman spectrum of an orthorhombic cassiterite inclusion in tetrahedral cassiterite from Slavkovský les. Laser power: 29 mW on the sample.

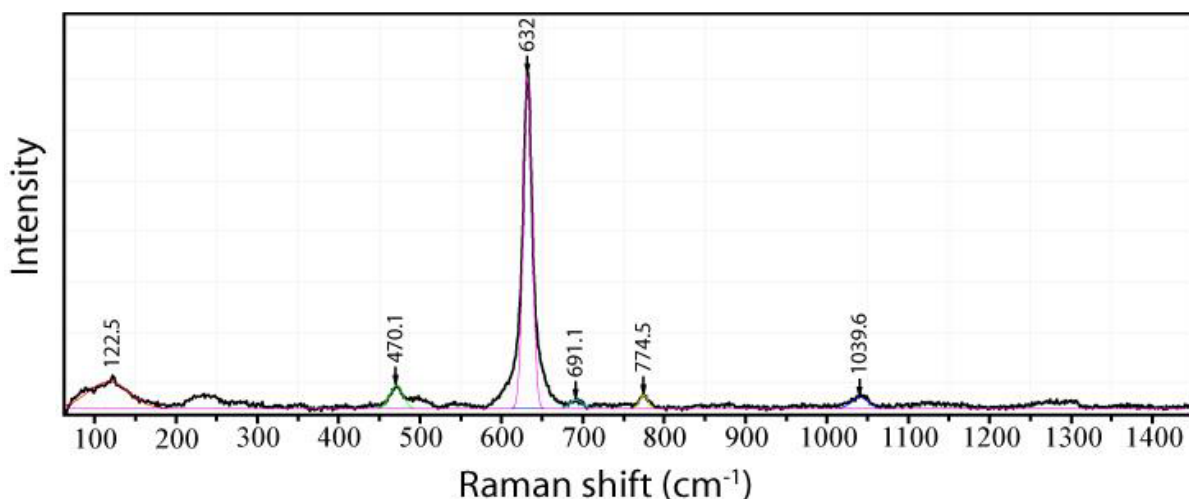


Figure 5: Tetragonal cassiterite (host) beside the orthorhombic cassiterite from Slavkovský les (see Figure 4). Laser power: 29 mW on the sample.

Interpretation

Helwig et al. (2003) [12] present in Figure 7 the pressure dependence of Raman frequencies through the rutile to CaCl₂-type cassiterite transition. Here, Figure 6 shows a similar, simplified relationship constructed from data from Hellwig et al. (2003) and Girão (2018) [12,13].

The exact position of the lines in Figure 6 depends on different conditions: temperature [14], crystal size (single crystals or nanoparticles), the disorder in SnO₂ [13], pressure media, as well as the laser energy on the sample. Because the structure changes in nature from the CaCl₂ to the rutile phase is a second-order transition (see Gupta et al. 2012), this transition is accompanied by minimal volume changes, by which the determination of the precise transition pressure is challenging. In addition, the cooling history in nature has undoubtedly had a significant influence (Table 2).

For the pressure P (in GPa), the following general equation is valid: $P = (\omega - a)/b$, with ω the corresponding Raman position at pressure. The value ω is the measured Raman band. For B_{1g}^{*} and A_g^{*}, are the following equations for the pressure (in GPa) valid:

$$B_{1g}^*: P(\text{GPa}) = 18.454 - 0.0408 * \omega - 0.000877 * \omega^2 \text{ (from 0 to 15 GPa).}$$

$$A_g^*: P(\text{GPa}) = 16.614 - 0.0515 * \omega + 0.000686 * \omega^2 \text{ (from 15 to 30 GPa).}$$

The weak and broad bands S1 and S2 correspond, according to Dieguez et al. (2001) [14], to the nanoparticle size.

In Figure 6, the red (E_g) and purple lines are corresponding lines generated maybe by different temperatures (see Diéguez et al. 2001)

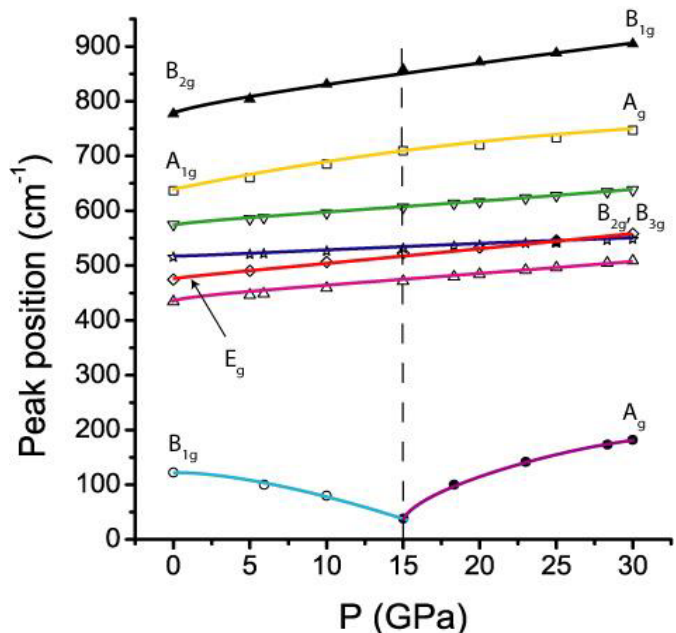


Figure 6: Schematic pressure (P) dependence of the Raman shift (cm⁻¹) through the rutile- to CaCl₂-type cassiterite transition. The dashed perpendicular line marks the phase transition (according to Hellwig et al. (2003) [12] and Girão (2018) [13]). The Raman modes are from Hellwig et al. (2003) [12], and the non-marked lines are from Girão (2018) [13].

Table 2: Peak position at ambient pressure and their pressure dependencies according to Hellwig et al. (2003) [12], Girão (2018) [13], and Girão et al. (2018) [3].

Rutile-type cassiterite			CaCl ₂ -type cassiterite			Authors
Mode	a	b	Mode	a	b	
E _g	474.7	3.21	B _{2g} , B _{3g}	483.0	2.5	Hellwig et al. (2003) [12]
A _{1g}	636.3	4.9	A _g	667.0	2.67	
B _{2g}	777.3	5.37	B _{1g}	807.5	3.25	
B _{1g} [*]	122.5		A _g [*]	100.0		Girão (2018) [13]
B _{2g}	774	4.0				
A _{1g}	633	4.6				
S1	575	2.1				
			A _g	434	2.5	Girão et al. (2018) [3]
E _g	475	3.3	B _{2g} , B _{3g}	-	-	
A _{1g}	634	4.8	A _g	~690	2.4	
B _{2g}	775	5.3	B _{1g}	~820	3.0	

[14] because both bands merge at low laser power on the sample. According to Gupta et al. (2013) [2], there are significant discrepancies between the phase transitions of the rutile-type cassiterite and CaCl₂-type cassiterite, depending on the used methods: 11.8 GPa from x-ray diffraction, 14.2 GPa from Raman spectroscopy, and 14.6 GPa from Brillouin spectroscopy.

From our Raman measurements, we obtain from the four typical Raman bands the following values (n – number of determinations):

$$\text{Mode } A_g \text{ } 117.8 \pm 13.5 \text{ cm}^{-1} \text{ (n=56): } P=20.1 \text{ GPa [12].}$$

$$\text{Mode } A_g \text{ } 444.8 \pm 2.6 \text{ cm}^{-1} \text{ (n=56): } P=4.3 \text{ GPa [3].}$$

$$\text{Mode } A_g \text{ } 438.4 \pm 3.1 \text{ cm}^{-1} \text{ (n=10 at 0.15 mW): } P=21.3 \text{ GPa [2]}$$

$$\text{Mode } E_g \text{ } 470,0 \pm 3.9 \text{ cm}^{-1} \text{ (n=43): } P=14.4 \text{ GPa [3]}$$

$$\text{Mode } B_{1g} \text{ } 834.8 \pm 0.7 \text{ cm}^{-1} \text{ (n=53): } P=23.4 \text{ GPa [2].}$$

Mode B_{1g} 829.1 ± 1.2 cm⁻¹ (n=10 at 0.15 mW): 17.5 ± 0.2 GPa (according to Gupta et al. 2012 [2].

A pressure of 16.8 ± 6.3 GPa results from 228 determinations, which demonstrates that the inclusions in rutile-type cassiterite with strong birefringence under crossed Nicols are CaCl₂-type cassiterite. The lower pressure for the 445 cm⁻¹ band (4.3 GPa, n=56) can be traced back to a faster transformation from the CaCl₂-type to the rutile-type cassiterite. Independent of the present state (remnants), the whole cassiterite was a primary CaCl₂-type cassiterite, as proved by the high number of “star-like” distributions of micrometer-large CaCl₂-crystals.

Discussion

The study of cassiterite samples from Slavkovský les in North Bohemia (Czech Republic) shows, in analogy to cassiterite from the Sauberg mine near Ehrenfriedersdorf/Saxonian Erzgebirge [4,5], clearly that some large cassiterite crystals contain remnants of CaCl₂-type cassiterite formed at pressures of about 15 GPa. This pressure corresponds to a depth of about 560 km (if the experimental data can be applied to nature). Together with the proof of mantle minerals

(diamond, lonsdaleite, moissanite, and others) in the upper crust (Greifenstein granite, Sauberg mine near Ehrenfriedersdorf, Annaberg granite, Sadisdorf, Zinnwald) the evidence of CaCl₂-type cassiterite in the Slavkovský les and Ehrenfriedersdorf tin mineralization give further solid hints to the direct interaction between deep mantle and crust via supercritical fluids/melts. The longstanding idea of Štemprok (see Figure 13 in Štemprok and Seifert, 2011 [15-17] added with ± vertical vein-like paths of supercritical fluids) is that significant amounts of tin of the Variscan Erzgebirge/Krušné hory and Slavkovský les come directly via supercritical fluids from the mantle region (mantle-derived fluids) find now new food for the mind. Furthermore, we have here the first confirmed case of pressure information from the untypical high-pressure CaCl₂-type cassiterite. Up to now, most information comes from mineral inclusions in diamonds.

Acknowledgment

For the cassiterite samples from the Erzgebirge/Krušné hory, I am grateful to Professor Ludwig Baumann (1929-2008) from the Mining Academy Freiberg. The author thanks Prof. Miroslav Štemprok (1933-2023) for many inspiring discussions during numerous field trips, meetings, and invited presentations in Prague.

References

- Balakrishnan K, Veerapandy V, Fjellvåg H, Vajeeston P (2022) First-principles exploration into the physical and chemical properties of certain newly identified SnO₂ polymorphs. *ACS Omega* 7: 10382-10393. [[crossref](#)]
- Gupta SD, Gupta SK, Jha PK, Ovsyuk NN (2013) A first principles lattice dynamics and Raman spectra of the ferroelastic rutile to CaCl₂ phase transition in SnO₂ at high pressure. *Raman J. Raman Spectroscopy* 44: 926-933.
- Girão HT, Hermet P, Masenelli B, Haines J, Mélinon P, Machon D (2018) Pressure induced sublattice disordering in SnO₂: Invasive selective percolation. *Physical Review Letters* 120: 265702-1 – 265702-6.
- Thomas R (2024) The CaCl₂-to-rutile phase transition in SnO₂ from high to low pressure in nature. *Geology, Earth and Marine Sciences* 6: 1-4.
- Thomas R (2023) Unusual cassiterite mineralization, related to the Variscan tin mineralization of the Ehrenfriedersdorf deposit, Germany. *Aspects in Mining & Mineral Science* 11: 1233-1236.
- Thomas R, Davidson P, Rericha A, Recknagel U (2022) Discovery of stishovite in the prismatine-bearing granulite from Waldheim, Germany: A possible role of supercritical fluids of ultrahigh-pressure origin. *Geosciences* 12: 1-13.
- Thomas R (1982) Ergebnisse der thermobarogeochemischen Untersuchungen an Flüssigkeitseinschlüssen in Mineralen der postmagmatischen Zinn-Wolfram-Mineralization des Erzgebirges. *Freiberger Forschungshefte C370*, Pg: 85.
- Thomas R, Davidson P, Rericha A, Recknagel U (2023) Ultrahigh-pressure mineral inclusions in a crustal granite: Evidence for a novel transcrustal transport mechanism. *Geosciences* 13: 1-13.
- Tuschel D (2012) Raman crystallography, in theory and in practice. *Spectroscopy* 27: 2-6.
- Lafuente B, Downs, RT, Yang H, Stone N (2015) The power of database: the RRUFF project. In: Armbruster T, Danisi RM (eds). *Highlights in mineralogical crystallography*. Berlin, 1-30.
- Hurai V, Huraiova M, Slobodnik M, Thomas R (2015) Geofluids – Developments in Microthermometry, Spectroscopy, Thermodynamics, and Stable Isotopes. *Elsevier* Pg: 489.
- Hellwig H, Goncharov AF, Gregoryanz E, Mao H, Hemley RJ (2003) Brillouin and Raman spectroscopy of the ferroelastic rutile to CaCl₂ transition in SnO₂ at high pressure. *Physical Review B* 67: 174110-1174110-7.
- Girão HT (2018) Pressure-induced disorder in bulk and nanometric SnO₂. *Material Chemistry, Theses, Université de Lyon*, Pg: 139.
- Diéguez A, Romano-Rodriguez A, Vilà A, Morante JR (2001) The complete Raman spectrum of nanometric SnO₂ particles. *Journal of Applied Physics* 90: 1550-1557.
- Štemprok M, Seifert T (2011) An overview of the association between lamprophyric intrusions and rare-metal mineralization. *Mineralogia* 42: 121-162.
- Štastný M, René M (2014) Argillization of topaz-bearing granites in the Hub Stock, Horni Slavkov-Krasno Sn-W ore district (Bohemian Massif, Czech Republic). *Acta Geodyn. Geomater* 11: 255-267.
- Thomas R, Trinkler M (2024) Monocrystalline lonsdaleite in REE-rich fluorite from Sadisdorf and Zinnwald/E-Erzgebirge, Germany. *Geology, Earth and Marine Sciences* 6(5), 1-6.

Citation:

Thomas R (2024) Rhomboedric Cassiterite as Inclusions in Tetragonal Cassiterite from Slavkovský les – North Bohemia (Czech Republic). *Geol Earth Mar Sci* Volume 6(5): 1-6.